SLAC-PUB-15679

Constraints on the Phase Plane of the Dark Energy Equation of State

Chien-Wen Chen*

Department of Physics, National Taiwan University,

Taipei 10617, Taiwan, R.O.C. and

Leung Center for Cosmology and Particle Astrophysics (LeCosPA),

National Taiwan University, Taipei 10617, Taiwan, R.O.C.

Pisin Chen

Kavli Institute for Particle Astrophysics and Cosmology,

SLAC National Accelerator Laboratory,

Menlo Park, CA 94025, U.S.A. and

LeCosPA, Department of Physics, and Graduate Institute of Astrophysics,

National Taiwan University, Taipei 10617, Taiwan, R.O.C.

Je-An Gu

LeCosPA, National Taiwan University, Taipei 10617, Taiwan, R.O.C.

Abstract

Classification of dark energy models in the plane of w and w', where w is the dark energy equation of state and w' its time-derivative in units of the Hubble time, has been studied in the literature. We take the current SN Ia, CMB and BAO data, invoke a widely used parametrization of the dark energy equation of state, and obtain the constraints on the w–w' plane. We find that dark energy models including the cosmological constant, phantom, non-phantom barotropic fluids, and monotonic up-rolling quintessence are ruled out at the 68.3% confidence level based on the current observational data. Down-rolling quintessence, including the thawing and the freezing models, is consistent with the current observations. All the above-mentioned models are still consistent with the data at the 95.4% confidence level.

*Electronic address: f90222025@ntu.edu.tw

Published in Phys.Lett.B682:267-273,2009 and arXiv:0905.2738.

Work supported in part by US Department of Energy under contract DE-AC02-76SF00515.

I. INTRODUCTION

Compelling evidence from different types of observation shows that the expansion of the universe is accelerating at late times (see [1] for a review). Within the framework of general relativity, this indicates that there should exist an energy source with significant negative pressure, termed dark energy, to drive this acceleration. The nature of dark energy is generally regarded as one of the most tantalizing problems in cosmology. Many dark energy models have been proposed and studied (see [1, 2], and references therein). While the cosmological constant remains the simplest realization of dark energy, current observations do not rule out the possibility of time-evolving dark energy [1]–[3].

In the pursuit of revealing the nature of dark energy, cosmological observations serve to constrain the behavior of dark energy. Theoretical studies, on the other hand, should determine whether dark energy models can be distinguished by their observational consequences. The ratio of pressure to energy density for dark energy, the equation of state $w = p/\rho$, is the characteristic of how the energy density evolves with time. The cosmological constant relates to the constant equation of state $w = -1$, while other dark energy models generally have time-evolving w. The time-derivative of w in units of the Hubble time, $w' = dw/dlna$, characterizes the dynamical behavior of the equation of state. Studies of the dynamical behaviors and classification of dark energy models in the w–w' phase plane have been carried out [4]–[8]. It is found that different dark energy models are bounded in different sectors in the w–w' plane.

In this paper, on the one hand, we gather the bounds for various dark energy models in the w–w' plane. On the other hand, we obtain the constraints on the w–w' plane in the redshift region $0 < z < 1$, by adopting a widely used parametrization [3, 9, 10], $w(z) = w_0 + w_a(1 - a) = w_0 + w_a z/(1 + z)$, based on the current observational data. The data set we use includes the recently compiled "Constitution set" of Type Ia supernovae (SN Ia) data [11]–[17], the cosmic microwave background (CMB) measurement from the five-year Wilkinson Microwave Anisotropy Probe (WMAP) [18], and the baryon acoustic oscillation (BAO) measurement from the Sloan Digital Sky Survey (SDSS) [19] and the 2dF Galaxy Redshift Survey (2dFGRS) [20]. We then compare the dark energy models with the constraints on the w–w' plane for $0 < z < 1$. The work close to ours is that of Barger et al. [21], in which they used the earlier data set and examined the dark energy models in the

w_0–w_a plane only at the redshift $z = 1$.

II. CLASSIFICATION OF DARK ENERGY MODELS

Quintessence

The quintessence model [22]–[24], which invokes a time-varying scalar field, generally allows its energy density and equation of state to evolve with time, and has $w > -1$. The equation of motion of the quintessence field is $\ddot{\phi} + 3H\dot{\phi} + V_{,\phi} = 0$, where $H = \dot{a}/a$ is the Hubble expansion rate, and $V_{,\phi} = dV/d\phi$. In terms of w and w', the equation of motion can be written as [25]

$$\mp \frac{V_{,\phi}}{V} = \sqrt{\frac{3(1+w)}{\Omega_\phi(a)}} \left[1 + \frac{1}{6}\frac{d\ln(x_q)}{d\ln(a)}\right], \tag{1}$$

where the minus sign corresponds to $\dot{\phi} > 0$ and the plus sign to the opposite, $\Omega_\phi(a)$ is the dimensionless energy density of the quintessence field, and $x_q = (1+w)/(1-w)$. For the down-rolling quintessence field ($\dot{V} < 0$), the left-hand side of Eq. (1) is positive, and the bound of w and w' can be obtained as $w' > -3(1-w)(1+w)$ [5, 6]. The up-rolling quintessence field ($\dot{V} > 0$) takes the other side, $w' < -3(1-w)(1+w)$. The bound of the tracker quintessence [26] is obtained in [5, 6]. However, strong acceleration today, with $w \lesssim -0.7$, requires the breakdown of tracking [7]. The bound should only apply to the high redshift [7], $z \gg 1$, which is not the region of interest in this paper. A conjectured limit of quintessence has been proposed in [7] as $V/(-V_{,\phi}) < M_P$, where M_P is the Plank mass. However, the physical origin of this limit is not clear [7]. We therefore do not impose this constraint on the quintessence model. Caldwell and Linder identified two categories of quintessence models, "thawing" and "freezing", based on their dynamical behavior [4]. For the thawing models, the equation of state is $w \approx -1$ at early times, but grows less negative with time as $w' > 0$. The bounds of the thawing models are $(1+w) < w' < 3(1+w)$. For the freezing models, initially the equation of state is $w > -1$ with $w' < 0$, but the field is frozen at late times where $w \to -1$ and $w' \to 0$. The bounds of the freezing models are $3w(1+w) < w' < 0.2w(1+w)$. Note that the upper bound for the freezing models is only valid for $z < 1$.

Phantom

The phantom model has negative kinetic energy and the equation of state $w < -1$ [27].

The equation of motion of the phantom field is $\ddot{\phi} + 3H\dot{\phi} - V_{,\phi} = 0$. In terms of w and w', the equation of motion can be written as [28]

$$\pm \frac{V_{,\phi}}{V} = \sqrt{\frac{-3(1+w)}{\Omega_\phi(a)}} \left[1 + \frac{1}{6}\frac{d\ln(x_p)}{d\ln(a)}\right], \tag{2}$$

where the plus sign corresponds to $\dot{\phi} > 0$ and the minus sign to the opposite, $\Omega_\phi(a)$ is the dimensionless energy density of the phantom field, and $x_p = -(1+w)/(1-w)$. For the up-rolling phantom field ($\dot{V} > 0$), the left-hand side of Eq. (2) is positive, and the bound of w and w' can be obtained as $w' < -3(1-w)(1+w)$. The down-rolling phantom field ($\dot{V} < 0$) takes the other side $w' > -3(1-w)(1+w)$. Note that Eq. (2) and the bounds are different from those obtained in [6].

Barotropic fluids

Barotropic fluids are those for which the pressure is an explicit function of the energy density, $p = f(\rho)$ (see [8] and references therein). The expression for w' can be written as [5, 8]

$$w' = -3(1+w)\left(\frac{dp}{d\rho} - w\right). \tag{3}$$

The sound speed for a barotropic fluid is given by $c_s^2 = dp/d\rho$. To ensure stability, we must have $c_s^2 \geq 0$, which gives the bound $w' \leq 3w(1+w)$ for non-phantom ($w > -1$) barotropic fluids [5, 8]. For causality, we further require $c_s^2 \leq 1$ [29], which gives the bound $w' \geq -3(1+w)(1-w)$ for $w > -1$ [8].

The classification of the above-mentioned dark energy models in the w–w' plane is shown in Fig. 1. Note that all of the bounds are valid at late times for $0 < z < 1$.

III. CONSTRAINTS ON THE w–w' PLANE

A. Observational data

We use the combined data set from three types of observations including the SN Ia observation, the CMB measurement, and the BAO measurement. We assume that the universe is flat in this paper.

We use the Constitution set of SN Ia data compiled by Hicken et al. [11]–[17], which provides the information of the luminosity distance and the redshift. The SN Ia samples lie

in the redshift region $0 < z < 1.55$. The luminosity distance-redshift relation is given by

$$d_L(z) = (1+z)\int_0^z \frac{dz'}{H(z')}. \tag{4}$$

We use the CMB shift parameter measured by the five-year WMAP observation [18],

$$R = \sqrt{\Omega_m H_0^2}\int_0^{1090.04} \frac{dz}{H(z)} = 1.710 \pm 0.019, \tag{5}$$

where H_0 is the Hubble constant and Ω_m is the dimensionless matter density at present. We use the BAO measurement from the joint analysis of the SDSS and 2dFGRS data [19, 20], which gives $D_V(0.35)/D_V(0.2) = 1.812 \pm 0.060$, where

$$D_V(z_{\rm BAO}) = \left[(1+z_{\rm BAO})^2 D_A^2(z_{\rm BAO})\frac{z_{\rm BAO}}{H(z_{\rm BAO})}\right]^{1/3}, \tag{6}$$

and $D_A(z)$ is the angular diameter distance,

$$D_A(z) = \frac{1}{1+z}\int_0^z \frac{dz'}{H(z')}. \tag{7}$$

To obtain the constraints on the w–w' plane, we invoke a broadly used form of parametrization of the equation of state [3, 9, 10],

$$w(z) = w_0 + w_a(1-a) = w_0 + w_a z/(1+z)\,. \tag{8}$$

The constraint of w_0, w_a and Ω_m is obtained by fitting the three parameters to this combined data set. The estimate of the parameters are found to be $w_0 = -0.89^{+0.12}_{-0.14}$, $w_a = -0.18^{+0.71}_{-0.74}$, $\Omega_m = 0.25^{+0.03}_{-0.02}$. The two-dimensional constraint of w_0–w_a is obtained and shown in Fig. 2.

B. Results of the constraints on the w–w' plane

We reconstruct the the w–w' plane via Eq. (8) and

$$w'(z) = -aw_a = -w_a/(1+z), \tag{9}$$

at late times for $0 < z < 1$. At each redshift, the two-dimensional constraint is obtained by converting the points on the boundaries of the confidence regions in the w_0–w_a plane to the corresponding points in the w–w' plane, following Eq. (8) and Eq. (9), for the 68.3% and

the 95.4% confidence regions respectively.[1] Since the transformation between (w, w') and (w_0, w_a) is linear, each point inside a confidence region in the w_0–w_a plane gives a distinct point inside the corresponding confidence region in the the w–w' plane.

In the w–w' plane, we find that the cosmological constant, the phantom models, the up-rolling quintessence models, and the non-phantom barotropic fluids lie outside the 68.3% confidence region in the redshift regions $0 < z < 1$, $0.18 < z < 0.22$, $0.4 < z < 1$ and $0.7 < z < 1$, respectively. This shows that the four models are ruled out at the 68.3% confidence level. On the contrary, the down-rolling quintessence models, including the thawing and the freezing models, overlap with the 68.3% confidence region for $0 < z < 1$. All of the models overlap with the 95.4% confidence region for $0 < z < 1$. Samples of the constraints on the w–w' plane at redshifts $z = 0$, 0.2, 0.7 and 1, together with the models, are shown in Fig. 3.

IV. TEST OF THE METHOD

In Sec. III B, we invoked a criterion that a model is ruled out at the 68.3% confidence level if for some redshift the model's corresponding sector in the w–w' plane does not overlap with the confidence region at all. To test the validity of this criterion and to address the concern about the inherent bias of the parametrization against certain models, we perform a Monte Carlo test of our method. The criterion is invalid if for some redshift the resulting 68.3% region from the Monte Carlo realization of the fiducial model does not overlap at all with the model's corresponding sector in the w–w' plane. We pick one or two fiducial models for each model category to test our method.

The fiducial models used in the test include *cosmological constant*: $w(z) = -1$, *thawing*: $w(z) = -0.82 + 0.23\ lna + 0.08\ (lna)^2$, *freezing*: $w(z) = -0.92 - 0.14\ lna - 0.05\ (lna)^2$, *up-rolling quintessence*: $w(z) = -1 + 0.0003\ a^{-6.4}$, *up-rolling phantom*: (a) $w(z) = -1.2$, (b) $w(z) = -1.16 - 0.2\ lna - 0.07\ (lna)^2$, *down-rolling phantom*: $w(z) = -1 - 0.0003\ a^{-7}$, and *none-phantom barotropic fluids*: $w(z) = -1 + 0.0035\ a^{-4}$. For all models, Ω_m is 0.25 and $w(z > 1.55)$ is equal to $w(z = 1.55)$. All models have $w(z) < -0.8$ for strong acceleration

[1] For the one-dimensional error propagation, following the reconstruction equations, the variance propagation is $Var(w) = \langle (w - \langle w \rangle)^2 \rangle = \langle [w_0 - \langle w_0 \rangle + (1-a)(w_a - \langle w_a \rangle)]^2 \rangle = Var(w_0) + (1-a)^2 Var(w_a) + 2(1-a)Cov(w_a, w_a)$ and $Var(w') = (-a)^2 Var(w_a)$.

today. The trajectories of the models in the w–w' plane are shown in Fig. 4 in the redshift region $0 < z < 1$.

In the test, we realize each fiducial model by simulating the SN Ia, the BAO and the CMB data assuming current data quality. 1000 sets of simulated data are generated and fitted with the three parameters w_0, w_a and Ω_m. The values of w_0 and w_a are converted to w and w' via Eq. (8) and Eq. (9) at each redshift. The 683 and the 954 of the 1000 Monte Carlo realizations, representing the 68.3% and the 95.4% region, are selected via their chi-square from the fiducial model.

As a result, the criterion passes the test for all the models, that is, for each model the corresponding sector overlap with the 68.3% Monte Carlo realized region in the w–w' plane in the redshift region $0 < z < 1$. Samples of the test results at redshifts $z = 0$, 0.4, 0.7 and 1 are shown in Fig. 5. It is seen that applying the criterion up to $z = 1$ might be pushing it to the limit, especially for the up-rolling quintessence, down-rolling phantom and the non-phantom barotropic fluid cases. Yet the conclusion that the three models are ruled out at the 68.3% confidence level in Sec. III B still holds if we apply the the criterion only for $0 < z < 0.7$.

V. CONCLUSION AND DISCUSSION

Applying the bounds for various dark energy models in the w–w' plane for redshift $0 < z < 1$, we find that several models including the cosmological constant, phantom, non-phantom barotropic fluids, and monotonic up-rolling quintessence are ruled out at the 68.3% confidence level based on the current observational data. On the other hand, down-rolling quintessence, including the thawing and the freezing models, is consistent with the current observations. All the models are still consistent with the data at the 95.4% confidence level. Using the same SN Ia data set, Shafieloo et al. [30] and Huang et al. [31] also found the cosmological constant inconsistent with the data at the 68.3% confidence level. Barger et al. [21] found the non-phantom barotropic fluids excluded at the 95.4% confidence level based on the earlier data set. We notice that there was a time the observations favored $w(z = 0) \leq -1$ [13] but now the observations favor $w(z = 0) \geq -1$. However, the conclusions are drawn at the 68.3% confidence level at most. It is hoped that the next-generation observations will constrain the dark energy equation of state an order of magnitude better [1, 3]. We shall be

able to identify dark energy at higher confidence in the coming future.

VI. ACKNOWLEDGMENT

C.-W. Chen is supported by the Taiwan National Science Council under Project No. NSC 95-2119-M-002-034 and NSC 96-2112-M-002-023-MY3, P. Chen by the Taiwan National Science Council under Project No. NSC 97-2112-M-002-026-MY3 and by US Department of Energy under Contract No. DE-AC03-76SF00515, and Gu by the Taiwan National Science Council under Project No. NSC 98-2112-M-002-007-MY3. All the authors thank Leung Center for Cosmology and Particle Astrophysics for the support.

---

[1] J. Frieman, M. Turner and D. Huterer, Ann. Rev. Astron. Astrophys. 46, 385 (2008) [arXiv:0803.0982 [astro-ph]].

[2] C. W. Chen, Je-An Gu and P. Chen, Mod. Phys. Lett. A 24, 1649 (2009) [arXiv:0903.2423 [astro-ph.CO]].

[3] A. Albrecht et al., arXiv:astro-ph/0609591.

[4] R. R. Caldwell and E. V. Linder, Phys. Rev. Lett. 95, 141301 (2005) [arXiv:astro-ph/0505494].

[5] R. J. Scherrer, Phys. Rev. D 73, 043502 (2006) [arXiv:astro-ph/0509890].

[6] T. Chiba, Phys. Rev. D 73, 063501 (2006) [arXiv:astro-ph/0510598].

[7] E. V. Linder, Phys. Rev. D 73, 063010 (2006) [arXiv:astro-ph/0601052].

[8] E. V. Linder and R. J. Scherrer, arXiv:0811.2797 [astro-ph].

[9] M. Chevallier and D. Polarski, Int. J. Mod. Phys. D 10, 213 (2001) [arXiv:gr-qc/0009008].

[10] E. V. Linder, Phys. Rev. Lett. 90, 091301 (2003) [arXiv:astro-ph/0208512].

[11] A. G. Riess et al. [Supernova Search Team Collaboration], Astrophys. J. 607, 665 (2004) [arXiv:astro-ph/0402512].

[12] P. Astier et al. [The SNLS Collaboration], Astron. Astrophys. 447, 31 (2006) [arXiv:astro-ph/0510447].

[13] A. G. Riess et al., Astrophys. J. 659, 98 (2007) [arXiv:astro-ph/0611572].

[14] G. Miknaitis et al., Astrophys. J. 666, 674 (2007) [arXiv:astro-ph/0701043].

[15] W. M. Wood-Vasey et al. [ESSENCE Collaboration], Astrophys. J. 666, 694 (2007) [arXiv:astro-ph/0701041].

[16] M. Kowalski et al., Astrophys. J. 686, 749 (2008) [arXiv:0804.4142 [astro-ph]].

[17] M. Hicken et al., arXiv:0901.4804 [astro-ph.CO].

[18] E. Komatsu et al. [WMAP Collaboration], Astrophys. J. Suppl. 180, 330 (2009) [arXiv:0803.0547 [astro-ph]].

[19] D. J. Eisenstein et al. [SDSS Collaboration], Astrophys. J. 633, 560 (2005) [arXiv:astro-ph/0501171].

[20] W. J. Percival, S. Cole, D. J. Eisenstein, R. C. Nichol, J. A. Peacock, A. C. Pope and A. S. Szalay, Mon. Not. Roy. Astron. Soc. 381, 1053 (2007) [arXiv:0705.3323 [astro-ph]].

[21] V. Barger, E. Guarnaccia and D. Marfatia, Phys. Lett. B 635, 61 (2006) [arXiv:hep-ph/0512320].

[22] R. R. Caldwell, R. Dave and P. J. Steinhardt, Phys. Rev. Lett. 80, 1582 (1998) [arXiv:astro-ph/9708069].

[23] Je-An Gu and W-Y. P. Hwang, Phys. Lett. B 517, 1 (2001) [arXiv:astro-ph/0105099].

[24] L. A. Boyle, R. R. Caldwell and M. Kamionkowski, Phys. Lett. B 545, 17 (2002) [arXiv:astro-ph/0105318].

[25] P. J. Steinhardt, L. Wang and I. Zlatev, Phys. Rev. D 59, 123504 (1999) [arXiv:astro-ph/9812313].

[26] I. Zlatev, L. M. Wang and P. J. Steinhardt, Phys. Rev. Lett. 82, 896 (1999) [arXiv:astro-ph/9807002].

[27] R. R. Caldwell, Phys. Lett. B 545, 23 (2002) [arXiv:astro-ph/9908168].

[28] J. Kujat, R. J. Scherrer and A. A. Sen, Phys. Rev. D 74, 083501 (2006) [arXiv:astro-ph/0606735].

[29] G. Ellis, R. Maartens and M. A. H. MacCallum, Gen. Rel. Grav. 39, 1651 (2007) [arXiv:gr-qc/0703121].

[30] A. Shafieloo, V. Sahni and A. A. Starobinsky, arXiv:0903.5141 [astro-ph.CO].

[31] Q. G. Huang, M. Li, X. D. Li and S. Wang, arXiv:0905.0797 [astro-ph.CO].

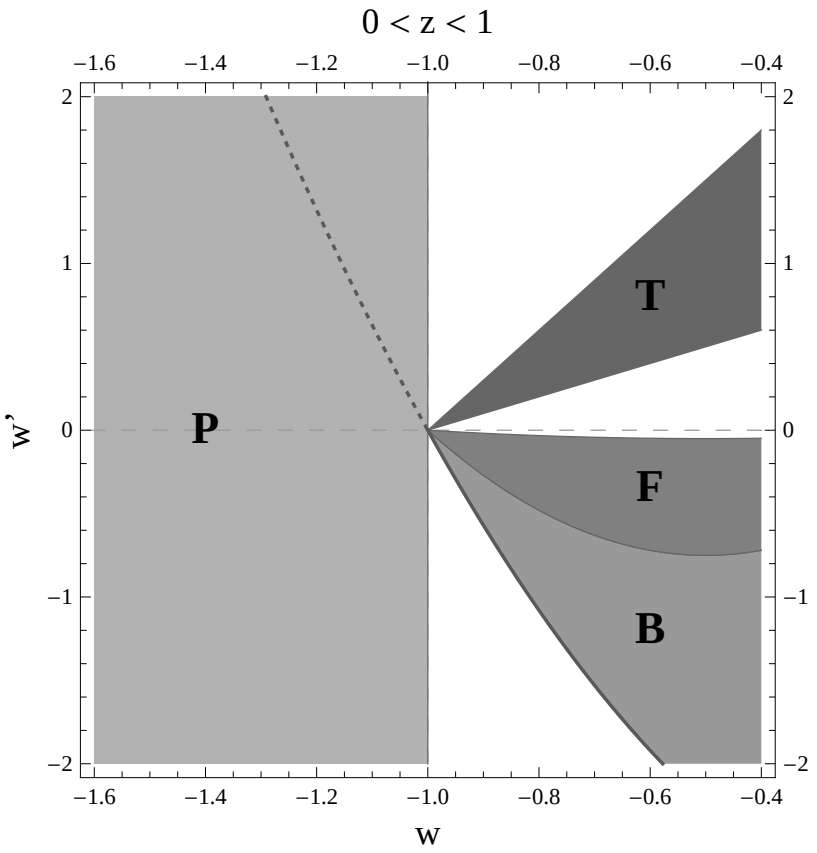

FIG. 1: Classification of dark energy models in the w–w' plane. Models are separated by the solid curves. The symbols "T", "F", "B", and "P" denote the "thawing", "freezing", "non-phantom barotropic", and "phantom" models, respectively. The quintessence models correspond to the region for $w > -1$. The cosmological constant corresponds to the point $(-1, 0)$. The bold solid curve is both the lower bound for the non-phantom barotropic models and the bound that separates the down-rolling and up-rolling quintessence models (down-rolling takes the upper side). The dotted curve is the bound that separates the down-rolling and up-rolling phantom models (up-rolling takes the lower side).

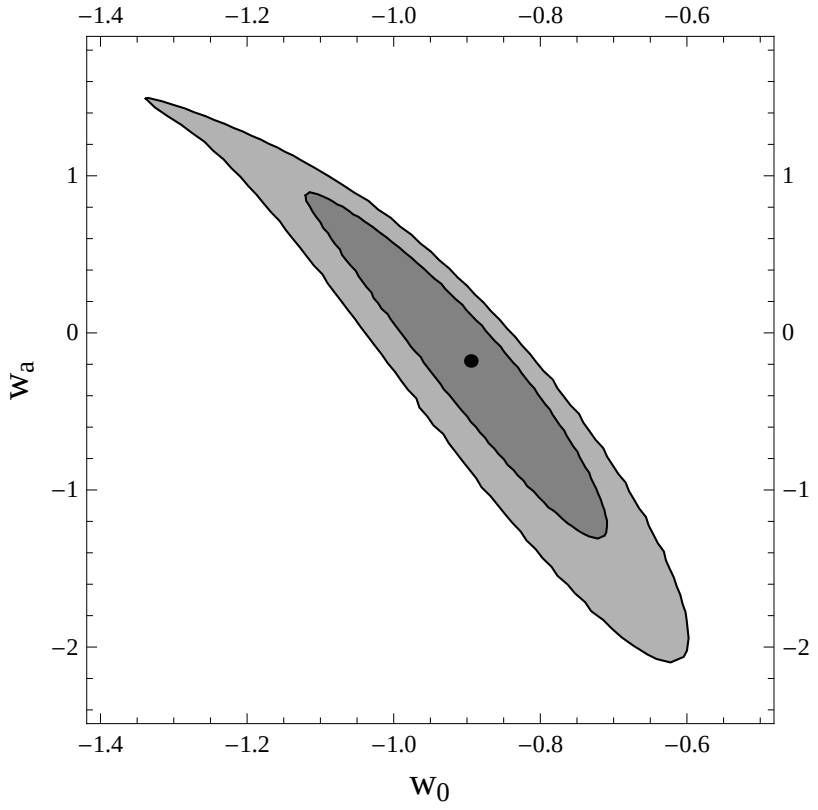

FIG. 2: The two-dimensional constraint of w_0–w_a based on the combined data set including the Constitution set of SN Ia data, the CMB measurement from the five-year WMAP, and the BAO measurement from the SDSS and 2dFGRS. The dark and the light gray areas correspond to the 68.3% and the 95.4% confidence regions, respectively. The black point denotes the best-fit values.

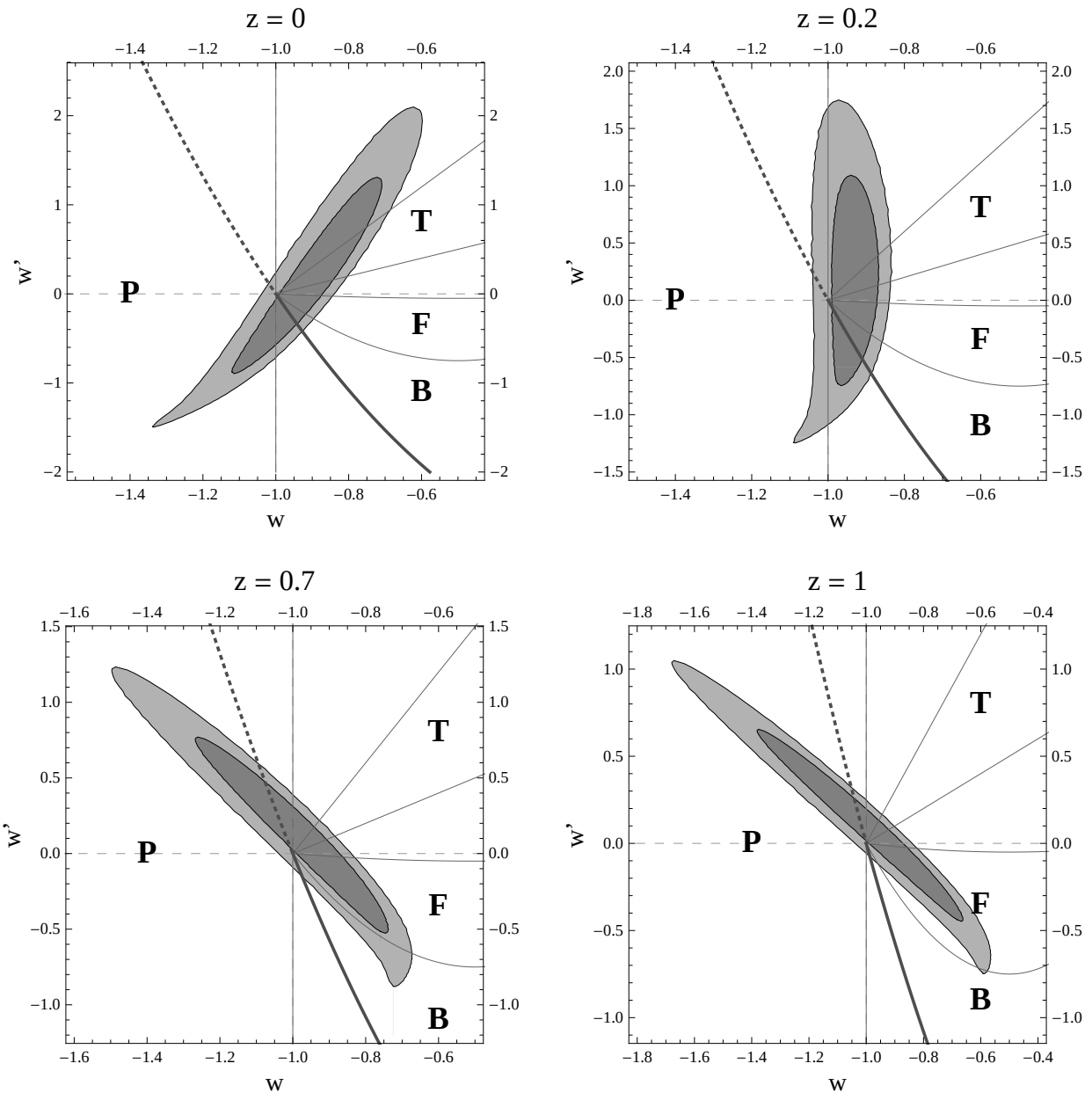

FIG. 3: Samples of the constraints on the w–w' plane at redshifts $z = 0$, 0.2, 0.7 and 1. The dark and the light gray areas correspond to the 68.3% and the 95.4% confidence regions, respectively. See the caption in Fig. 1 for the description of the regions to that the models belong. The cosmological constant lie outside the 68.3% confidence region at all of the redshifts. The down-rolling phantom models lie outside the 68.3% confidence region at $z = 0$ and $z = 0.2$. All the phantom models lie outside the 68.3% confidence region at $z = 0.2$. Both the up-rolling quintessence models and the non-phantom barotropic fluids lie outside the 68.3% confidence region at $z = 0.7$ and $z = 1$. The down-rolling quintessence models including the thawing and the freezing models overlap with the 68.3% confidence region at the four redshifts. All of the models overlap with the 95.4% confidence region at the four redshifts.

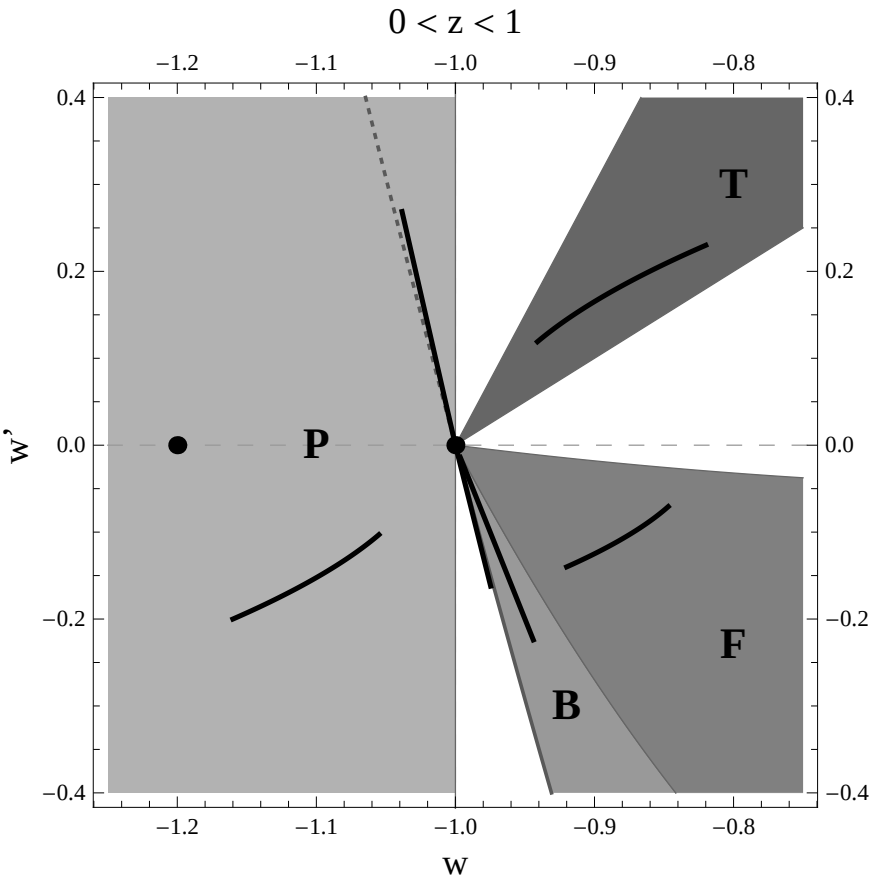

FIG. 4: Trajectories of the fiducial models for the test in the redshift region $0 < z < 1$. See the text in Sec. IV for the description of the models. The trajectories are shown by the black points and the black curves.

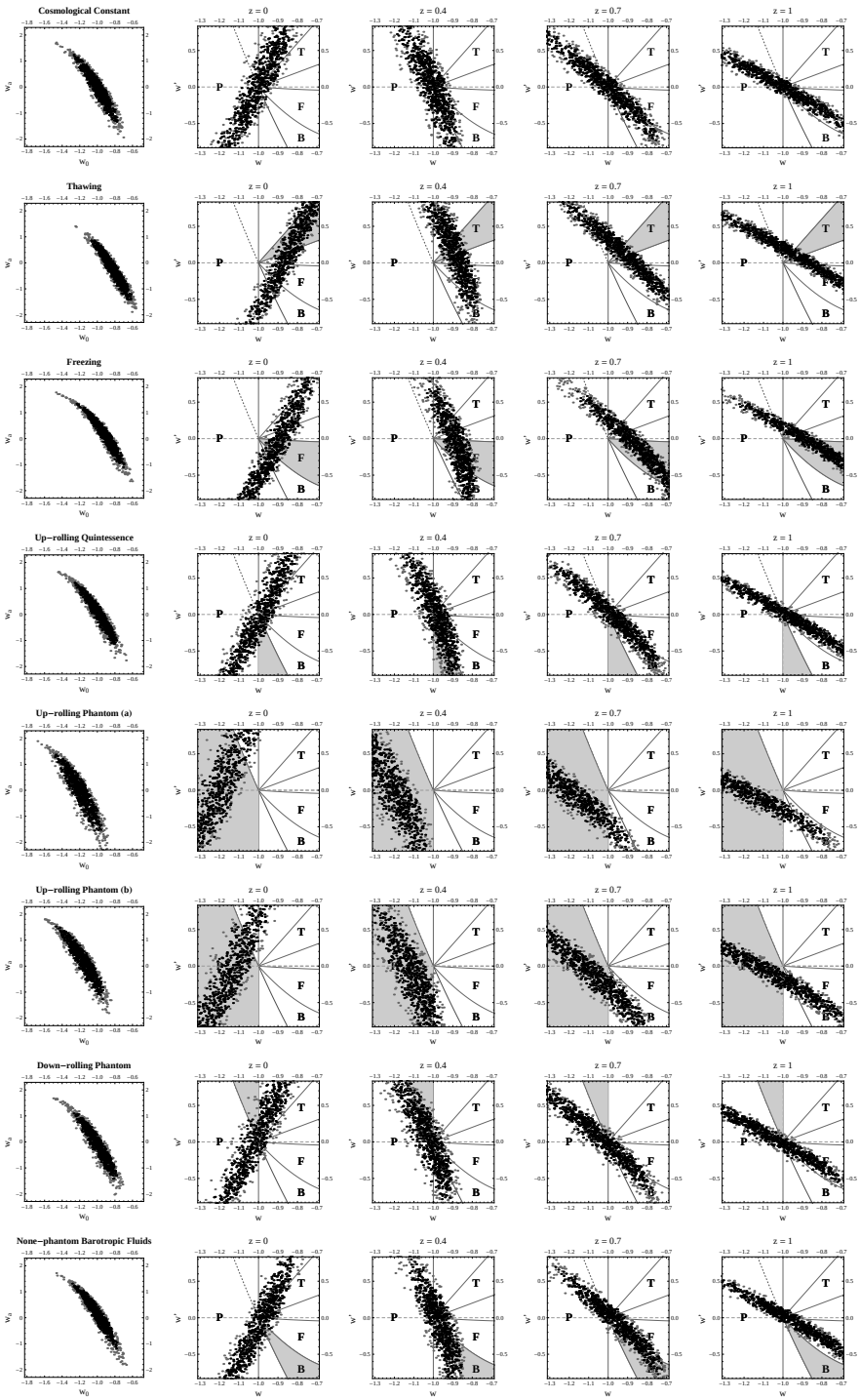

FIG. 5: Samples of the Monte Carlo test results of the method. From the first to the eighth row are the results corresponding to the fiducial models of cosmological constant, thawing, freezing, up-rolling quintessence, up-rolling phantom (a) and (b), down-rolling phantom and non-phantom barotropic fluids, respectively. The first column is the w_0–w_a plane and the rest four are the w–w' plane at redshifts $z = 0$, 0.4 0.7 and 1. The 68.3% Monte Carlo realized region is represented by the black points, while the 95.4% by the black and the dark grey points. The corresponding sectors of the fiducial models are filled with the light grey color. See Sec. IV for discussion.